Experiments in a cylindrical magnetic shock tube

By G. C. VLASES

Guggenheim Aeronautical Laboratories, California Institute of Technology

(Received 2 November 1962)

Experiments have been carried out in a cylindrical magnetic shock tube on the propagation of a shock wave into a fluid containing a uniform transverse magnetic field. Cylindrical shock waves in the Mach number range from 20 to 100 have been produced which are very stable and reproducible. Theory predicts basic differences between the case where the gas is initially highly conducting (pre-ionized) and the case where a gas-ionizing shock propagates into a cold gas. Good agreement between theory and experiment has been obtained for the gas ionizing shocks.

1. Introduction

This paper concerns an experimental investigation of the magneto-hydrodynamic analogy to a classical piston problem in ordinary gas dynamics and is an extension of some previously reported work (Liepmann & Vlases 1961). The experiment involves driving a 'magnetic piston' into a field in the presence of a transverse magnetic field. The fluid may either be conducting ahead of the shock or may be made conducting by the passage of the shock.

The experimental geometry employed was first described by Anderson *et al.* (1958), and was suggested independently by Liepmann. Current passes through a solid copper centre conductor (figure 1) and returns in a hollow cylindrical arc through the gas. The interaction of the B_θ field produced by the current in the centre conductor with the returning current produces a Lorentz force, or, equivalently, a magnetic pressure, which acts radially outward in the manner of a solid cylindrical piston expanding with time and drives a shock wave into the ambient gas. The device may thus be termed a cylindrical magnetic shock tube. An axial field B_{z_0} is established prior to the discharge. It is the interaction of the wave motion with the axial field that is of primary interest here.

There are several features inherent in this device which make it useful for shock studies. The most important of these are the stability and repeatibility of the flow. This gross stability, which makes the experiments feasible, has been extensively studied by Colgate & Furth (1960) and others and will not be further discussed. In addition, a great deal of theoretical work has been done on idealized models of the flow and provides a guide for the interpretation of experimental results. Other features include low wall losses and accessibility of the advancing front for measurements.

By varying B_{z_0} and other parameters in the problem, the ratio of ion cyclotron frequency ω_{c_i} to collision frequency ν can be carried through a wide range, making possible an investigation of both the 'collisionless shock' limit and the collision-

dominated cases as well as the transition from one to the other. This paper deals mainly with flows in which $\omega_{ci}/\nu \ll 1$.

In § 2 various theoretical models for the shock tube are discussed. § 3 describes the experimental apparatus; and § 4 is concerned with the experimental results and conclusions.

2. Theoretical predictions of shock tube performance

It is assumed throughout that the conductivity in the arc is sufficiently high that the current runs in a relatively thin annular region, and the concept of a localized 'magnetic piston' therefore has validity. This assumption is fairly well justified *a posteriori* by the experimental results. Single-fluid theory (magnetohydrodynamics) is used except when it is clearly inadequate; recourse is then taken to a more elaborate description.

The nature of the flow will be seen to depend critically on whether or not the fluid ahead of the shock is appreciably conducting. For that reason the theoretical discussion is divided into two sections; the first describing the motion when the fluid is initially highly conducting throughout the chamber, and the second describing flows in which a very strong shock propagates into an essentially non-conducting gas.

Most of the experiments reported here have been done without any attempt at pre-ionization. There are two reasons, however, for discussing both theoretical models here. First, experiments are currently being carried out in which the gas is rendered highly conducting before the main discharge, and preliminary results indicate that the 'everywhere highly conducting' theory is applicable. Secondly, in the absence of attempted pre-ionization, the gas ahead of the shock may become more or less conducting due to radiation and electron diffusion through the shock front (McLean *et al.* 1960; Wiese, Berg & Griem 1961; McLean, Kolb & Griem 1961).

Shock moving into a conducting fluid

The simplest theoretical model is a gross balance of rate-of-change of momentum against pressure, suggested by Rosenbluth, and described frequently as snowplough theory. It is assumed that the piston moves into the fluid and sweeps it up into a very thin, dense layer on the piston surface. For a cylindrical piston the equation of motion is (Greifinger & Cole 1961)

$$\frac{d}{dt}\left(\pi r_c^2 \rho_0 \frac{dr_c}{dt}\right) = 2\pi r_c [p_{m_\theta} - p_{m_z}], \tag{1}$$

where r_c is the piston radius, ρ_0 is the ambient gas density, and p_{m_θ} and p_{m_z} are the magnetic pressures, $B^2/2\mu$, of the azimuthal and axial fields. In this equation, the radius of the inner conductor and the ambient gas pressure are assumed negligible compared to the shock radius and magnetic pressure. For the case $B_{z_0} = 0$ and $I = I_0\,\omega t = V_0 t/L$, where V_0 and L are the initial condenser voltage and average inductance of a slightly damped RLC circuit, equation (1) possesses the conical similarity solution $r_c = u_0 t$, where

$$u_0 = \left\{\frac{V_0^2}{L^2}\frac{\mu}{8\pi^2\rho_0}\right\}^{\frac{1}{4}}, \tag{2}$$

and will be called the characteristic snowplough velocity. For $B_{z_0} \neq 0$ it is found that the solution is again conical, $r_c = u_c t$, where u_c is related to u_0 and to the Alfvén speed in the ambient fluid b_0 by

$$\left(\frac{u_c}{u_0}\right)^2 = -\left(\frac{b_0}{2u_0}\right)^2 + \left[\left(\frac{b_0}{2u_0}\right)^4 + 1\right]^{\frac{1}{2}}. \tag{3}$$

Clearly $u_c/u_0 < 1$ and the piston is retarded by the axial field.

As was shown by Greifinger & Cole, snowplough theory is equivalent to the Newtonian limit in ordinary gasdynamics and thus can be expected to represent the flow only in the case of very strong shocks. A shock wave is termed strong when it propagates with a speed large compared to the speed of corresponding infinitesimal disturbances. In the present instance, the latter speed is the combined wave speed $c = \sqrt{(a_0^2 + b_0^2)} \approx b_0$ for $a_0/b_0 \ll 1$. Thus, increasing the axial field while holding the other parameters of the problem fixed is equivalent to raising the generalized acoustic speed and hence to weakening the shock. We therefore expect a breakdown in the snowplough theory for sufficiently high values of B_{z_0}.

An exact solution for the cylindrical magnetic shock tube was found by Greifinger & Cole (1961) using the full magnetohydrodynamic equations. In their solution, the current was assumed to rise linearly and the conductivity was taken to be everywhere infinite. The main results of that solution, which of course possesses conical similarity, are as follows. (i) Equation (3) predicts the speed of the piston with remarkable accuracy even for very weak shocks, but is very inadequate for predicting the velocity of any shocks other than very strong ones. (ii) For a fixed u_0 the shock speed *increases* and the piston speed decreases (according to equation (3)) as B_{z_0} increases, accompanied by a decrease in compression of the plasma across the shock. (The rate of increase of shock speed with B_{z_0} is less than the rate of increase of acoustic speed with B_{z_0} so that the shock Alfvén Mach number approaches 1.) (iii) The axial magnetic field increases in passing through the shock proportionately to the density increase, a consequence of flux conservation through a contour attached to the fluid.

In the experiments the glass chamber wall is surrounded by coils which produce the axial field. During the short time of the experiment, these coils appear somewhat to the advancing wave motion as an infinitely conducting cylinder which might be expected to influence the electric and magnetic fields and hence the fluid motion. It is important to note that in the case considered here of a very highly conducting fluid, there can be no disturbance (either electromagnetic or fluid-mechanical) ahead of the shock (Whitham 1959); hence the wall has no effect until the first shock reaches it. An effect does arise, however, from the top and bottom electrodes. Being highly conducting, they tend to anchor the B_z field lines and cause them to become convex near the electrodes as the shock propagates outward. This effect has been minimized by extensive radial slotting of the electrodes.

We now consider the situation where the conductivity is appreciable throughout the chamber but not infinite. In this case two new effects appear, diffusion of the magnetic fields through the fluid, and ohmic heating.

At the shock front the diffusion of the induced azimuthal current is counter-

balanced by the non-linear breaking effect familiar in shock motion, resulting in a steady profile whose thickness is determined by the transport coefficients. In these experiments, the width is of order $(\mu\sigma)^{-1}$ since the magnetic diffusivity is the largest of those involved.

The structure of magnetohydrodynamic shocks has been studied by Marshall (1955) and others. When the shock thickness is governed by conductivity, two types of profiles occur. For high field strengths, all the variables undergo transition in a length of order $(\mu\sigma)^{-1}$; for sufficiently low fields there exists a sharp thermodynamic shock at the end of the magnetic field transition region. Thus one sees a sharp Rankine–Hugoniot shock with a long tail on the low pressure side. In a cylindrical geometry, the jump conditions must be appropriately modified if the thickness of the shock is not small compared to the radial position of the shock.

Diffusion of the field into the plasma also occurs at the plasma-vacuum interface (piston) and there the diffusion depth grows continuously as $t^{\frac{1}{2}}$ since there is no counteracting mechanism. However, from considerations of conservation of mass it is clear that the separation between the shock and the piston grows as t, so the shock should separate cleanly from the diffusing piston for sufficiently large t.

The effect of Ohmic heating is to produce a non-constant-velocity wave system, that is, to destroy the conical similarity. For example, if one imagines that most of the heating occurs near the centre during the initial stages of the discharge when the conductivity is likely to be quite low, then conditions are approximated for the classical blast wave solution where the velocity decays as $1/r$. Therefore, the deviation from constant velocity experimentally determined may provide a measure of the relative importance of heating and magnetic pushing.

Propagation of shock waves into a non-conducting fluid

In this section we choose as a model a shock propagating into a non-conducting fluid in which there is an axial field B_{z_0}. The shock is assumed to be sufficiently strong that the gas becomes highly conducting a short distance behind it. The essential point is that now the field must be continuous through the shock and hence the jump conditions are the ordinary Rankine–Hugoniot relations (Burgers 1957). This does not mean there is no effect of the field on the flow, for body forces arise in the region of the piston tending to retard the piston and thus produce a *slower* shock rather than the faster shock produced by the field when the fluid is everywhere highly conducting. However, the shocks are strong shocks since their strength depends on the ordinary Mach number. Thus, a snowplough theory remains valid for predicting the shock motion.

For the case of no wall, equation (3) is again valid for describing the piston path and the flow remains conical.

In contrast to the model discussed above, the effect of a conducting wall around the chamber is now important, since electromagnetic disturbances *can* propagate ahead of the shock because the damping mechanism is absent.

Consider the idealized problem of a highly conducting, thin, hollow, cylindrical piston advancing with velocity u into a vacuum region surrounded by a fixed,

highly conducting cylindrical wall (e.g. a coil producing the B_{z_0} field). There is initially a uniform field in the vacuum region. Solution of Maxwell's equations, with boundary conditions which include putting $(E-uB)$ equal to zero on both the piston and the wall, shows that the flux is conserved in the annular region between the piston and wall as the piston advances. Thus the field in front of the piston is compressed from its original value B_{z_0} to the value $B_{z_0}[1-(r_c/R)^2]$, where r_c and R are the piston and wall radii, respectively.

To apply these results to the present experiment one must reconcile two questions. First, the coils do not close on themselves but are connected to an external circuit. However, the driving capacitors are short circuited during the passage of the shock across the chamber. Secondly, there are gaps between adjacent coils so that some of the field 'leaks out' instead of being compressed between the piston and the wall; the experiments show that about 25 % of the flux is so lost (see § 4).

Therefore we apply this idealized model to our experiment and equation (1) becomes

$$\frac{d}{dt}\left\{x^2\frac{dx}{dt}\right\} = \frac{x}{R^2\rho_0}\left[\frac{\mu I(t)^2}{4\pi^2R_0^2x^2} - \frac{B_{z_0}^2}{\mu(1-x^2)^2}\right], \tag{4}$$

where $x = r_c/R$. For $I(t) \sim t$ and $B_{z_0} = 0$ the solution is again $r_c = u_0 t$. For $B_{z_0} \neq 0$, however, the piston slows down as it approaches the wall, even for a linearly rising current. That is, conical similarity is destroyed in this case by the presence of the conducting wall. The situation is now analogous to flow over a convex body rather than a cone (Liepmann & Vlases 1961).

In summary, we see that the flow pattern is quite different when the shock advances into a non-conducting fluid rather than into one which is a good conductor. In the former case the shock speed increases but its strength drops; in the latter, the shock travels more slowly but remains relatively strong.

In the foregoing discussion of expected shock tube performance the existence of an idealized fluid with scalar conductivity has been assumed. In fact, of course, the fluid is composed of electrons, ions, and neutrals, and this will become important in understanding some of the experimental results. In particular, the detailed mechanism by which the current and field interact and a shock is produced depends on three-fluid effects and is not completely understood at the present time.

3. Experimental apparatus and techniques

Basic discharge chamber

A schematic view of the discharge chamber and the circuitry is shown in figure 1. The chamber is approximately 4 in. long and $6\frac{1}{2}$ in. inside diameter; the diameter of the centre teflon insulator is $\frac{5}{16}$ in. The main discharge current is supplied by two 15 μF capacitors in parallel and the quarter cycle of the discharge is 4·5 μsec. Most tests are run at 12 kV, corresponding to a peak current of 123 kA.

The axial magnetic field is produced by discharging a 1000 μF bank at up to 4 kV through a four-coil system of the type described by Barker (1949). It reaches its peak value (up to 12 kG) in 940 μsec and is then short-circuited. In

this arrangement of coils the spacing and relative currents in the inner and outer coil pairs are chosen to give maximum field uniformity in a short cylindrical region. Because the field is pulsed, extensive radial slotting of the top and bottom circular stainless-steel electrodes is necessary to permit establishment of a uniform field. With slotted electrodes the uniformity is better than 5 % over most of the chamber.

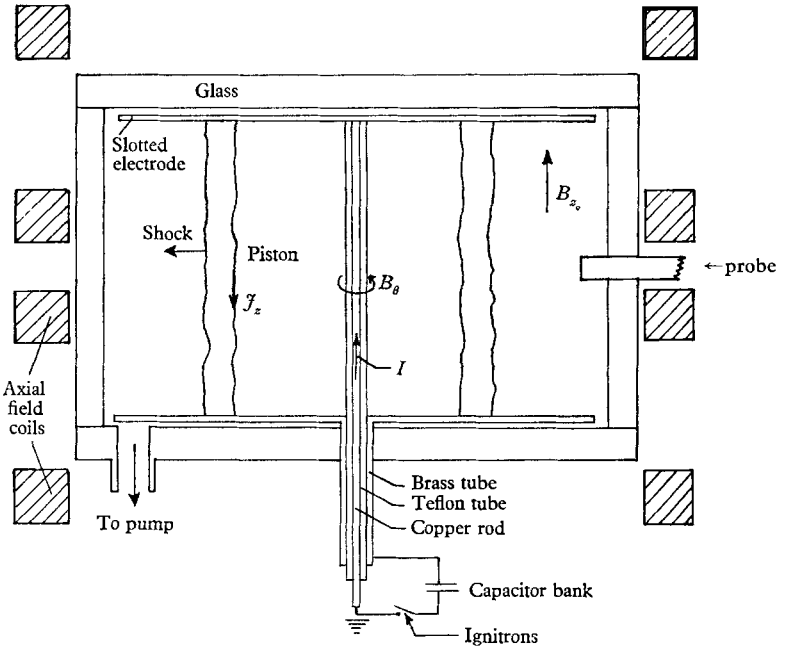

FIGURE 1. Schematic diagram of apparatus.

Instrumentation

On each firing the condenser-bank voltage is monitored as a function of time with a capacitance-type voltage divider for use as a time reference.

It seemed desirable at the outset of the investigation to develop instrumentation which would detect directly the existence of a sharp pressure pulse in the fluid so that questions concerning the relative positions of light fronts, current fronts, and shock waves could be clarified. To this end pressure probes employing barium titanate crystals on the front (discharge end) of the probe were constructed. The crystal and conducting parts of the probe are shielded from the discharge by encasing them in glass. This creates matching problems due to the differing acoustical impedances of the glass and crystal so that the probes detect the arrival of a pulse but do not produce a faithful pressure-time history. The initial voltage output caused by a shock striking the probe has been crudely calibrated as a function of Mach number and initial pressure in a conventional shock tube. The rise time attainable depends primarily on the crystal thickness only and is 0·2 μsec for the 1 mm crystals used here. Probes in which the crystal is mounted at the rear of a long rod leading out of the discharge chamber were

tried and quickly discarded due to the relatively long rise time (of the order of 1μsec at best) caused by wave dispersion in the rod.

Time derivatives of magnetic fields ($\dot{B}_\theta$, $\dot{B}_z$) are measured with small search coils (1 mm inner diameter, 10 turns) encased in a Pyrex envelope inserted radially into the discharge. For sufficiently high conductivities, a glass shield is known to have a deleterious effect on probe response (Camac *et al.* 1961; Lovberg 1959). However, for the moderate conductivities encountered in the present experiment, the probes give an accurate measurement of the fields in the plasma (Lovberg 1959; Dippel & Teckenburg 1959). As a check on possible electrostatic effects, a grounded centre tap probe (Dippel & Teckenburg 1959) used in connexion with a differential preamplifier was used on several runs and yielded results identical to the single-coil probes.

A single-frame Kerr-cell camera made by Electro Optical Instruments, Inc., is used to take pictures through the side of the chamber at given times after the onset of the discharge. Exposure times are all either $\frac{1}{20}$ or $\frac{1}{10}\,\mu$sec.

A 'run' is accomplished by first discharging the B_z capacitor bank into the field coils and then firing the main bank after a suitable delay. A 'set' of experiments in a given gas at a particular initial pressure and condenser voltage consists of pressure, $\dot{B}_\theta$, $\dot{B}_z$, and the Kerr-cell records for six radial probe stations and five or more values of initial axial field B_{z_0}. Two probes were used, a pressure transducer and a search coil, each lying in the chamber mid-plane and separated azimuthally by 60°.

The results presented below deal primarily with sets of experiments in argon and helium at 100 and 500μHg initial pressure with all other parameters fixed. Although most of the experiments were done without pre-ionization, some preliminary experiments with pre-ionization will be described.

4. Experimental results and interpretations

Experiments without pre-ionization

In this section, emphasis is placed on three sets of experiments which illustrate most of the important features.

Table 1 presents some of the relevant parameters. The equilibrium temperature behind the shock ($T_{2\text{eq.}}$) is calculated from Rankine–Hugoniot relations and equilibrium thermodynamics using the observed shock speeds for $B_{z_0} = 0$ and serves as a rough estimate of conditions behind the shock. It is possible, of course, that thermodynamic equilibrium is not established sufficiently quickly to make the calculation strictly applicable. (Extrapolation of the results of Petschek & Byron 1957 indicates that equilibrium would be reached (in argon) in a time between $\frac{1}{2}$ and 1μsec. The electric field will tend to keep the electrons hotter, enhancing the ionization rate but tending to prevent the establishment of true thermodynamic equilibrium.) The equilibrium degree of ionization behind the shock ($\alpha_{2\text{eq.}}$) is based on $T_{2\text{eq.}}$ and p_2 and is defined as the number of electrons per original neutral particle. The electrical conductivity is obtained from Spitzer's (1956) result for fully ionized gases. The diffusion depth δ_c of the driving field B_θ into the gas in the time required to traverse the chamber R/u_0 is also listed,

from which it is seen that the 'piston' is somewhat diffuse, and a clean separation of the shock and piston is not to be expected.

In scanning table 1, one should note that a major effect of the axial field is to decrease the shock strength and hence to produce less conductivity and consequently greater departures from the idealized model.

The state of the plasma is such that, except in a few extreme cases, $\omega_{c_i}/\nu < 1$; that is, the condition for a 'collisionless shock' is not fulfilled.

Relative front positions

Typical (r, t)-diagrams are shown in figures 2, 3 and 4. The legend needs a little further clarification. Circles represent the arrival of a sharp pressure pulse. Triangles indicate the arrival at a given radius of a peak in the function $\dot{B}_\theta(r_i, t)$, which for sharp peaks (ideal flow) correspond closely to the maximum current density j_z; i.e. to the arrival of the magnetic piston at the distance r_i. The symbols labelled '$\dot{B}_z$ null' refer to the null in $\dot{B}_z(r_i, t)$ which occurs when compression of the axial field at a given radius is complete. This, according to the theoretical discussion given above, should correspond closely to the shock position. Finally the solid circles represent the radius of the luminous front. Where deviations from cylindrical symmetry were observed, the positions of the left- and right-hand sides of the front are both shown.

These figures illustrate the relative positions of the various fronts. In helium at 500 μ the shock precedes the piston as one expects. This is true both with and without the axial field. The separation between the fronts changes little with field strength, indicating a non-magnetohydrodynamic shock flow. For no field the light front is with the shock, while it lags slightly when a field is applied. Figure 3 illustrates a result which at first appears somewhat anomalous. For $B_{z_0} = 0$ the piston appears to be slightly ahead of the shock, while for $B_{z_0} = 4950$ the 'piston' is definitely *ahead* of the shock. It should be recalled that the 'piston' is really a relatively thick annular region in which volume currents flow, rather than a current sheet at a well-defined location (see figures 10 and 11 below). Thus, the shock is located near the rear of the current-carrying region in argon (figure 3) and near the front in helium (figure 2). Figure 4 shows that a similar tendency for the piston to precede the shock occurs in argon at 100 μ, although it is not pronounced. It is also clear that the light front tends to stay near the shock wave in all cases.

A possible explanation of the piston 'preceding' the shock can be given as follows. Because they carry most of the current, the electrons are the primary recipients of the Lorentz force acting on the gas. Thus they tend to move away from the ions which are pulled along behind them by the electrostatic force arising from the charge separation which occurs. As the ions are heavier, they are more effective in transferring energy to the neutrals and the principal 'shock' disturbance is associated with the ions. The separation which can be maintained between electrons and ions depends in part on the relative ease with which the electrons and ions can move through the neutrals, as well as on the product of the Debye length times the Mach number. (Since the electron concentration varies by several orders of magnitude in passing through the shock

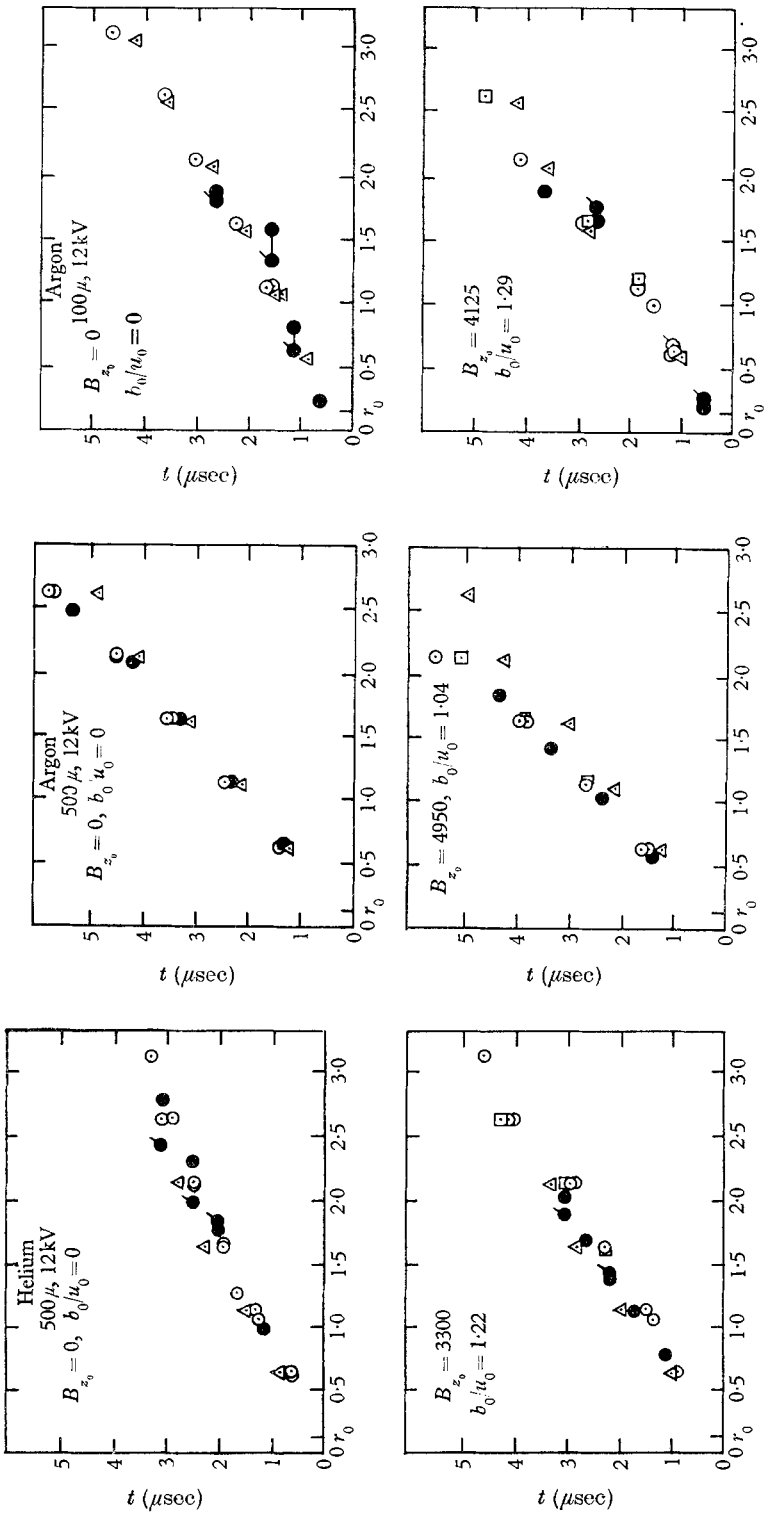

FIGURE 2

FIGURE 3

FIGURE 4

FIGURES 2–4. Relative positions of magnetic piston, light front, and shock front in helium and argon at 500 and 100 μ initial pressure. The plotted points are: ⊙, pressure probe; △, $\dot{B}_\theta$ peak; □, $\dot{B}_z$ null; ●, light front, right side; ◐, light front, left side.

region, the Debye length is difficult to determine even approximately.) Now the electron-atom collision cross-sections for helium and argon are quite different in the energy range of 1–3 eV which is characteristic of these experiments. The electron-atom cross-section for argon as a function of energy displays a very pronounced dip at 1 eV (Ramsauer effect) to a value less than $\frac{1}{6}$ that of

Experiment	B_{z_0} (G)	b_0/u_0	$T_{2eq.}$ (°K)	$\alpha_{2eq.}$	σ_2 (mho/m)	δ_c (cm)
Argon, 100 μ, 12 kV;	0	0				
$u_0 = 1{\cdot}95$ cm/μsec;	1,350	0·42				
$M_0 = 60$	2,750	0·86	≈ 30,000	Doubly ionized	13,000	1·6
	4,125	1·29				
	5,500	1·72				
Argon, 500 μ, 12 kV;	0	0				
$u_0 = 1{\cdot}30$ cm/μsec;	1,650	0·35				
$M_0 = 40$	3,300	0·69	≈ 23,000	Nearly double	8,750	2·3
	4,950	1·04				
	6,600	1·38				
Helium, 100 μ, 12 kV;	0	0				
$u_0 = 3{\cdot}47$ cm/μsec;	680	0·38				
$M_0 = 34$	1,350	0·75	21,900	0·68	8,000	1·5
	2,050	1·14				
	2,700	1·53				
Helium, 500 μ, 12 kV;	0	0				
$u_0 = 2{\cdot}32$ cm/μsec;	1,100	0·41				
$M_0 = 22{\cdot}7$	2,200	0·82	19,500	0·25	7,000	2·0
	3,300	1·22				
	4,350	1·61				

TABLE 1

helium, whose electron-atom cross-section is approximately independent of energy in this range (Massey & Burhop 1952). It then increases rapidly, becoming equal to that of helium at around 4 eV. From table 1 it is seen that the characteristic temperature in argon at 500 μ for no axial field is about 2 eV. The presence of a field slows the shock (see below) and moves the temperature towards 1 eV, where the cross-section is the smallest; this is precisely where the largest separation of the fronts occurs. The experiments in argon at 100 μ correspond to a cross-section intermediate between that of the experiments in helium at 500 μ, where the piston lags as in a normal shock-piston flow, and argon at 500 μ. As seen in figure 4, the relative positions of the fronts in this case are consistent with the above reasoning.

While the foregoing explanation is certainly an over-simplification of a complicated phenomenon, it appears clear that the Ramsauer effect plays an important role. A great deal of work remains to be done before the process whereby a magnetic piston drives a gas and produces a shock wave is thoroughly understood.

Kerr-cell photographs

Several interesting features of the flow are shown in figures 5 (plate 1) and 6 (plate 2). As is evident, the light front is straighter and more clearly defined at high initial pressures. In argon, with no axial field applied, small offshoots or flares of luminosity are present which disappear when even a slight initial field is used. In general, the effect of the presence of the axial field is to enhance the stability of the luminous front.

A slight tendency was noted, particularly in argon without an applied B_z field, for the radius of the cylindrical light front at a given time to be slightly greater at the cathode than at the anode. Most of the luminosity is due to line radiation from excited states and thus the light front corresponds closely to the ionization front and shock, as is apparent from figures 2–4. The tilting is believed to be due to a tendency of the ions to migrate toward the cathode and in so doing to drift slowly outward; the effect disappears in the presence of an axial field.

Some curvature of the light front near the electrodes due to the anchoring of the field lines is observed, but the effect is quite small.

Shock properties

Figures 7–9 illustrate the influence of axial field strength on the motion of the shock and piston. In each case, the shock is *slowed* by the axial field. This fact in itself is fairly conclusive evidence that the shock is an ordinary one propagating into an essentially non-conducting fluid, as discussed in § 2 above. The increasing deviation from conical similarity as the field increases indicates further that the effect of the conducting wall (coils) is being felt. Note that although the shock slows down in fairly good agreement with snowplough theory, the velocity of the piston follows a peculiar behaviour as described above. An approximate solution to equation (4) has been obtained by expanding in a power series to find the behaviour near the origin, and by equating the inertial term to zero to find the behaviour near the wall ($x = 1$). The results are plotted as a dotted line on figure 8, from which it is seen that equation (4) closely predicts the shock motion.

As the shock slows, the pressure jump must drop. Calibration of the pressure probes in an ordinary shock tube shows that the output is roughly proportional to the reflected shock pressure jump. For strong shocks, this is proportional to the square of the shock Mach number, so that output falls rapidly as the shock speed drops. Comparison of figure 10 with figures 7 and 9 shows this to be experimentally verified.

Plots of rB_θ are given in figures 10 and 12 for a typical set of runs. The circles indicate the position of the shock at a given time. The slope of these curves is an indication of the piston current, $j_z = (r\mu)^{-1}\partial(rB_\theta)/\partial r$. (The curves were not differentiated because of the inherent inaccuracy arising from measuring the field at only six radial stations.) As can be seen, the current front travels all the way to the wall for no axial field, but is effectively stopped by the presence of an initial field and diffuses toward the wall through the cold gas as time progresses. It is clear that the field acts to limit compression of the gas.

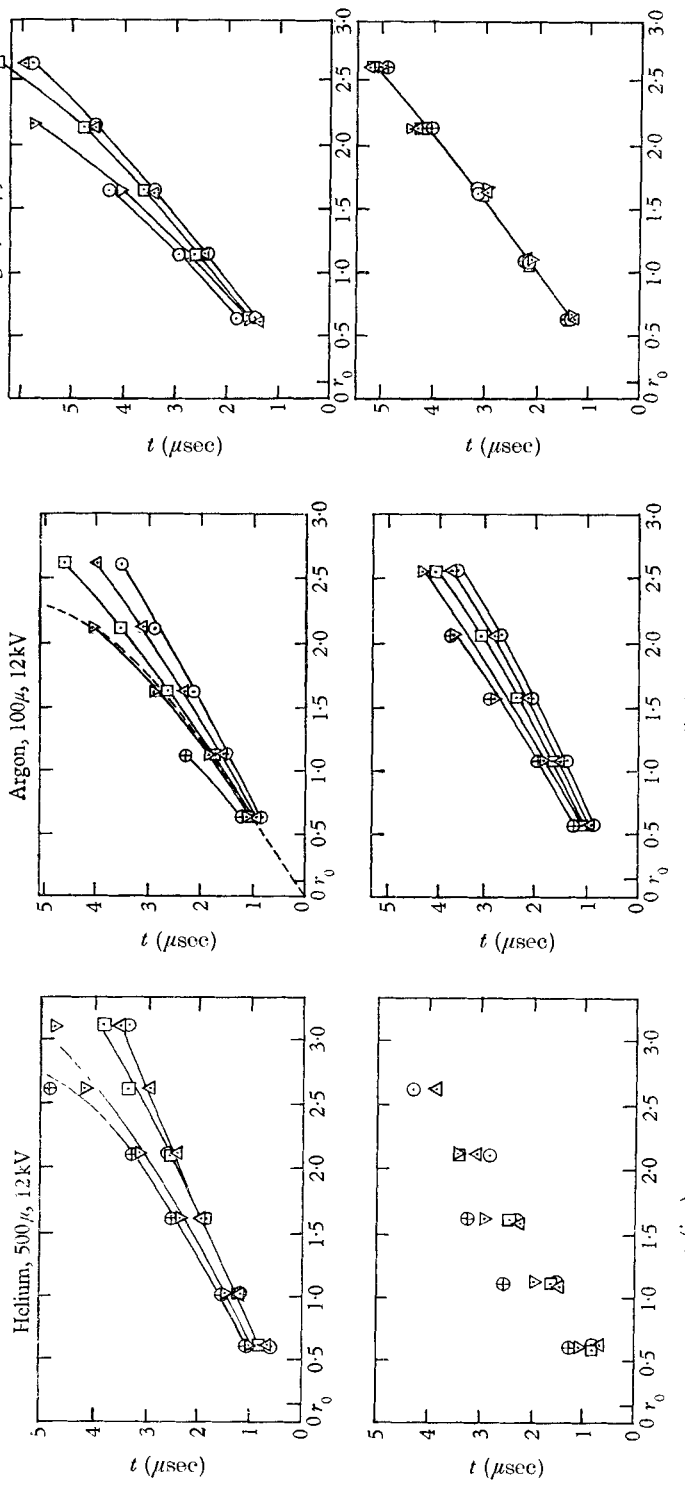

FIGURE 7

FIGURE 8

FIGURE 9

FIGURES 7–9. Effect of axial magnetic field strength on shock and piston velocities. Figure 7: ⊙, $\sim B_{z_0} = 0$; △, $\sim B_{z_0} = 1100$; □, $\sim B_{z_0} = 2200$; ▽, $\sim B_{z_0} = 3300$; ⊕, $\sim B_{z_0} = 4350$. Figure 8: ⊙, $\sim B_{z_0} = 0$, $b_0/u_0 = 0$, △, $\sim B_{z_0} = 1350$, $b_0/u_0 = 0{\cdot}42$; □, $\sim B_{z_0} = 2750$; $b_0/u_0 = 0{\cdot}86$; ▽, $\sim B_{z_0} = 4150$, $b_0/u_0 = 1{\cdot}29$; ⊕, $\sim B_{z_0} = 5500$, $b_0/u_0 = 1{\cdot}72$; ---, equation (4) $b_0/u_0 = 1{\cdot}29$. Figure 9: ⊙, $\sim B_{z_0} = 0$, $b_0/u_0 = 0$; △, $\sim B_{z_0} = 1650$; $b_0/u_0 = 0{\cdot}35$; □, $\sim B_{z_0} = 3300$, $b_0/u_0 = 0{\cdot}70$; ▽, $\sim B_{z_0} = 4950$, $b_0/u_0 = 1{\cdot}04$; ⊕, $\sim B_{z_0} = 6600$, $b_0/u_0 = 1{\cdot}38$. The upper graphs refer to the arrival of the pressure pulse, the lower graphs to the arrival of the $\dot{B}_\theta$ peak.

In conclusion, these experiments without pre-ionization indicate that an ordinary shock propagates into a relatively non-conducting fluid at a rate governed by the speed of the magnetic piston, whose motion is retarded by the presence of an axial field. The shock is associated mainly with the ions, which appear to be driven electrostatically by the electrons.

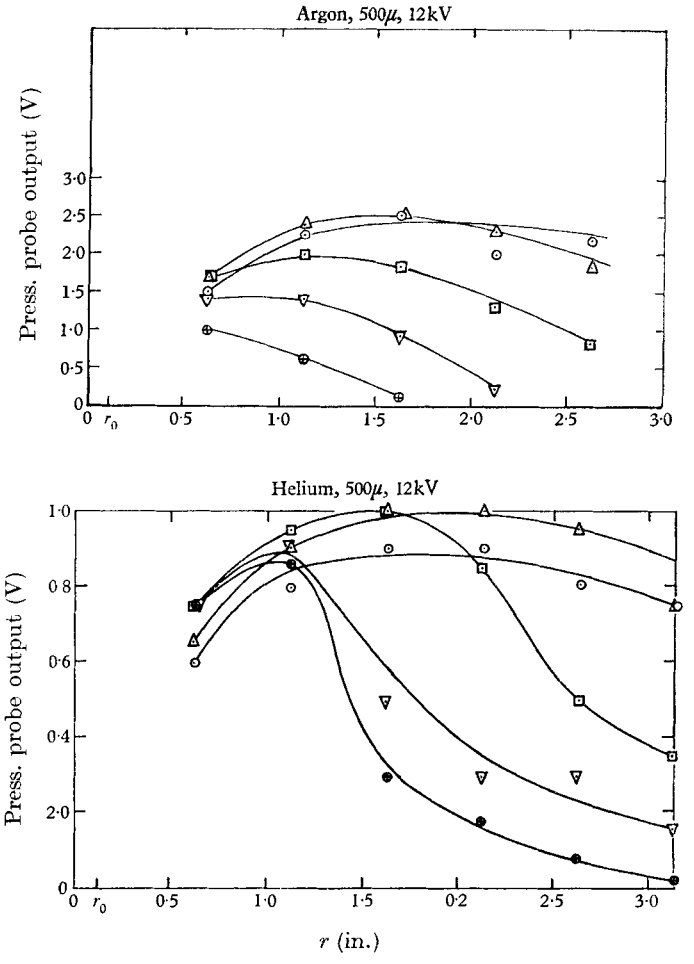

FIGURE 10. Variation of pressure probe output with radius. Argon: ⊙, $\sim B_{z_0} = 0$; △, $\sim B_{z_0} = 1650$; ⊡, $\sim B_{z_0} = 3300$; ▽, $\sim B_{z_0} = 4950$; ⓘ, $\sim B_{z_0} = 6600$. Helium: ⊙, $\sim B_{z_0} = 0$; △, $\sim B_{z_0} = 1100$; ⊡, $\sim B_{z_0} = 2200$; ▽, $\sim B_{z_0} = 3300$; ⊕, $\sim B_{z_0} = 4350$.

Experiments with pre-ionization

In order to produce a true magnetohydrodynamic shock of thickness small compared to chamber dimensions, an equilibrium condutivity ahead of the shock of the order of 10^4 mho/m is required. Shock heating seems to be the most direct way of accomplishing this in these experiments. The simplest scheme is simply to examine the shock motion emanating from the second half-cycle of the main discharge. This has been done, and preliminary experiments indicate that the

shock is speeded up by the presence of the field, i.e. the wave is actually a magnetohydrodynamic shock wave. The difficulty with this procedure is twofold: (1) the state of the fluid and the magnetic field into which the second shock propagates is not precisely known since it follows the first so quickly; and (2) at the present time the instrumentation severely limits the accuracy of measurements on the second shock. Work is currently in progress which uses two separate inverse pinches fired at an arbitrary delay with respect to each other, the first one providing a high equilibrium conductivity throughout the chamber, and the second one being the subject of investigation. Further results will be reported as they become available.

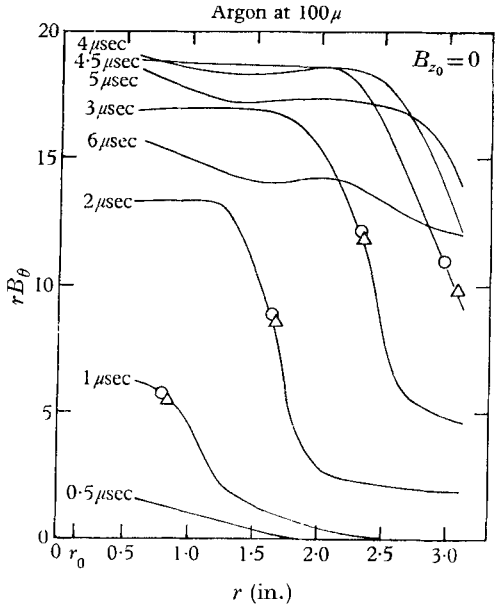

FIGURE 11. Typical rB_θ profiles in argon. $B_{z_0} = 0$.

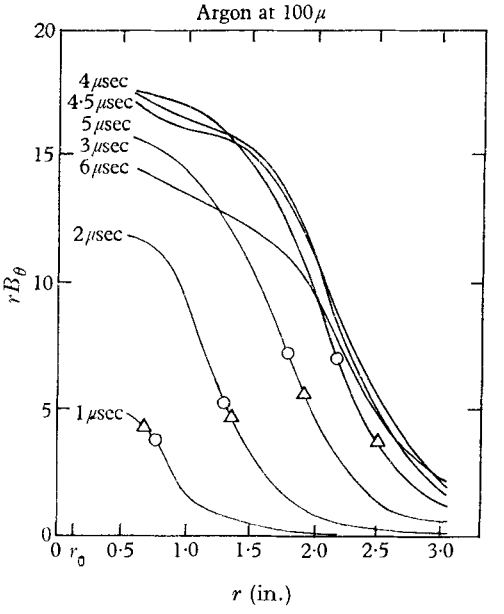

FIGURE 12. Typical rB_θ profiles in argon. $B_{z_0} = 4125$; $b_0/u_0 = 1{\cdot}29$.

This work was supported by the Francis I. du Pont Fund and by a National Science Foundation Graduate Fellowship. The author is indebted to Prof. H. W. Liepmann for suggesting this problem and for his guidance during the course of the work. He also wishes to thank Prof. J. D. Cole and G. B. Whitham for their many helpful discussions.

REFERENCES

ANDERSON, O. A. *et al.* 1958 *Phys. Fluids*, **1**, 489.

BARKER, J. R. 1949 *J. Sci. Inst.* **26**, 273.

BURGERS, J. M. 1957 *Univ. of Maryland Tech. Note* no. BN-102.

CARMAC, M. *et al.* 1961 *AVCO Research Rep.* no. 107.

COLGATE, S. A. & FURTH, H. P. 1960 *Phys. Fluids*, **3**, 982.

DIPPEL, K. H. & TECKENBURG, W. 1959 *Proc. 4th Int. Conf. on Ionization Phenomena in Gases*. North Holland Publishing Co.

GREIFINGER, C. & COLE, J. D. 1961 *Phys. Fluids*, **4**, 527.

LIEPMANN, H. W. & VLASES, G. 1961 *Phys. Fluids*, **4**, 927.

LOVBERG, R. H. 1959 *Ann. Phys.* **8**, 311.

MARSHALL, W. 1955 *Proc. Roy. Soc.* A, **233**, 367.

MASSEY, H. S. W. & BURHOP, E. H. S. 1952 *Electronic and Ionic Impact Phenomena.* Oxford University Press.

MCLEAN, E. A. *et al.* 1960 *Phys. Fluids*, **3**, 982.

MCLEAN, E. A., KOLB, A. C. & GRIEM, H. R. 1961 *Phys. Fluids*, **4**, 1055.

PETSCHEK, H. & BYRON, S. 1957 *Ann. Phys.* **1**, 270.

SPITZER, L. Jr. 1957 *Physics of Fully Ionized Gases.* New York: Interscience.

WHITHAM, G. B. 1959 *Commun. Appl. Math.* **12**, 113.

WIESE, W., BERG, H. F. & GRIEM, H. R. 1961 *Phys. Fluids*, **4**, 250.

FIGURE 5. Kerr-cell photographs in argon, taken approximately 2·5 μsec after initiation of the discharge. Anode is at top. Exposure time 0·5μsec. Initial voltage 12 kV.

(*Facing p.* 96)

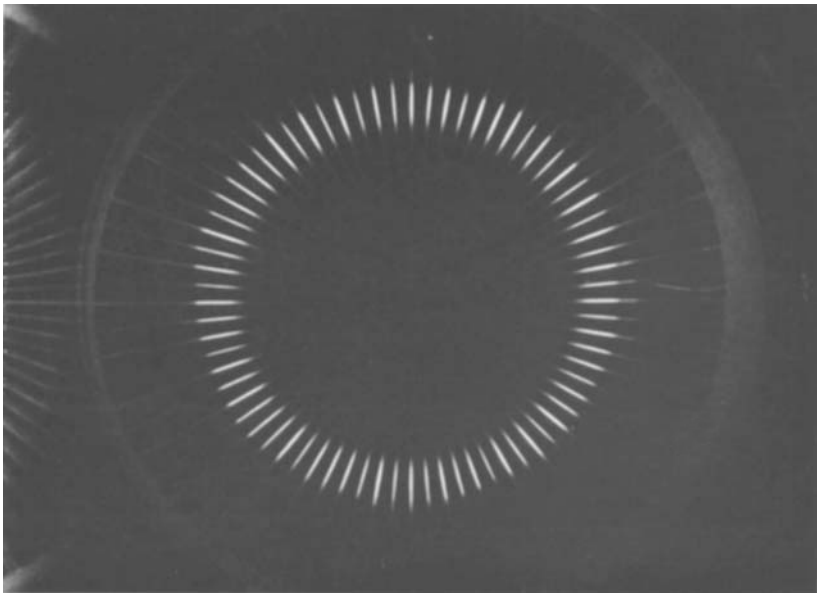

(*a*) $B_{z_0} = 0$

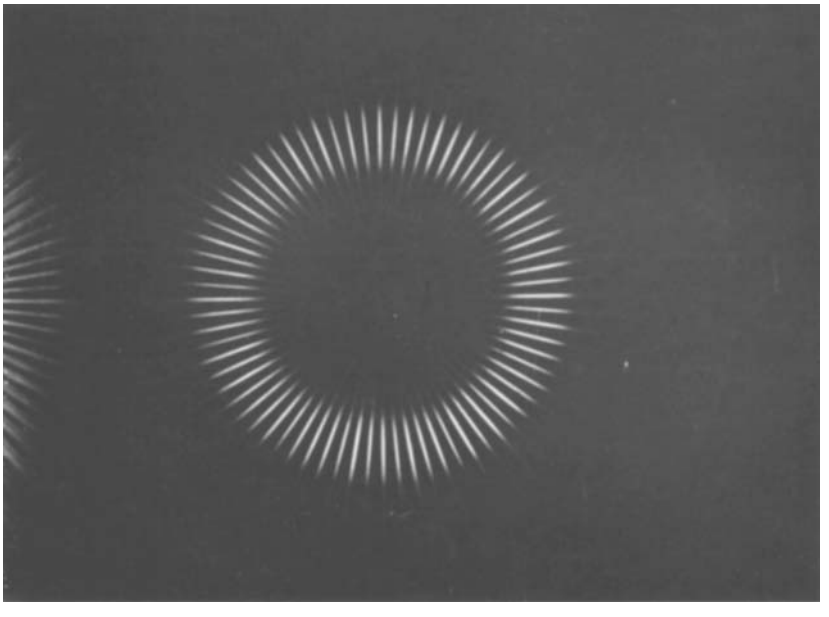

(*b*) $B_{z_0} = 4950$ G

FIGURE 6. Kerr-cell photographs in argon taken through top electrode (anode) at approximately 4·5 μsec after discharge. Exposure time 0·05 μsec. Initial voltage 12 kV. Initial pressure 500 μ. Note the high degree of symmetry. (Extraneous light on the left side of the photos arises from reflections.)